Renewable Energy 66 (2014) 150–158

Contents lists available at ScienceDirect

Renewable Energy

journal homepage: www.elsevier.com/locate/renene

Flexible TCO-free counter electrode for dye-sensitized solar cells using graphene nanosheets from a Ti–Ti(III) acid solution

Kai-Hsiang Hung, Chin-Hao Chan, Hong-Wen Wang*

Department of Chemistry, Center for Nanotechnology, Chung-Yuan Christian University, Chungli 320, Taiwan, ROC

ARTICLE INFO

Article history:
Received 14 May 2013
Accepted 2 December 2013
Available online 22 December 2013

Keywords:
Titanium
Ti(III) ion
Graphene
Dye-sensitized solar cell

ABSTRACT

A rapid and simple route to synthesize highly conductive graphene-based nanosheets for use as a flexible counter electrode in dye-sensitized solar cells is presented. The flexible counter electrode is free of transparent conductive oxide layer, i.e., TCO-free. A clean graphene with high quality is obtained by the chemical reduction of graphene oxide (GO) using titanium metallic powders in a hydrochloric acid solution. The Ti^{+3} ions that dissociated from metallic Ti particles in a hydrochloric acid solution result in a clean graphene material with no formation of TiO_2 nanoparticles, which are always present on graphene when only Ti^{+3} ions are used for the reduction, i.e., an anatase TiO_2 nanoparticle by-product will be always left on the graphene product when not using metallic Ti particles. The chemical reaction mechanisms for these differences are revealed in this report. The reduced materials are characterized by field emission scanning electron microscopy, high-resolution transmission electron microscopy, Raman spectroscopy, thermo-gravimetric analysis, Fourier transform infrared spectrometry, UV–vis spectroscopy and X-ray photoelectron spectroscopy. The four-point probe method is also employed to characterize the surface conductivity of the graphene films. This high quality graphene film exhibits comparable or better performance than those obtained using conventional sputtered Pt counter electrode when used as a flexible counter electrode of dye-sensitized solar cells.

1. Introduction

Dye-sensitized solar cells (DSSCs) comprise a dye-sensitized nanocrystalline titanium dioxide (TiO_2) electrode, organic sensitizers, liquid electrolytes, and platinum (Pt) counter electrode [1]. Typically, Pt counter electrodes in DSSCs have been prepared by vacuum deposition or thermal annealing of a Pt precursor on a transparent conductive oxide (TCO) substrate to reduce the I_3^- to I^- in redox electrolytes [1]. Although Pt has a high conductivity, catalytic activity and stability, Pt is one of the most expensive components in DSSCs, giving that the TCO is also expensive (about 60% of total cost). Therefore, the development of alternative materials for the Pt-free and TCO-free DSSCs is highly desired. Currently, graphene has been identified and demonstrated for this purpose successfully [2]. Graphene is a two-dimensional single layer of carbon atoms with a hexagonal close-packed structure [3]. It was successfully synthesized and isolated using the mechanical exfoliation of graphite by Geim et al., in 2004 [4]. Currently, there are many ways to synthesize graphene materials. Among them, oxidation-reduction in a chemical solution has become one of the most developed methods reported in the literature [5–9] due to its large scale production and cost-effectiveness. In these works, the graphitic oxide precursor has mostly been prepared by the method of Hummers and Offeman [5]. The reduction of this precursor is generally performed using reducing agents such as hydrazine and its derivatives, $NaBH_4$, or other toxic reagents [10–13]. A more environmentally friendly but time-consuming process (100 °C for 5 days) uses benzyl alcohol as the reducing agent [14]. Polymers and vitamin C were also employed as the reduction and dispersion agents; however, these materials inevitably remain in the solution with the graphene product [15–17]. An acidic solution, a KOH/NaOH solution, and UV irradiation also proved to be effective to reduce GO. However, the C/O ratio and the thermal stability of these graphene products were not high [18–20]. Intensive research has led to the use of metal or metallic ions in acid solution as advantageous reducing agents [21–29]. Zn, Fe, Pt, Pd or other ions were utilized to realize this purpose. An easy and advantageous preparation using $TiCl_3$ solution as the reducing agent has also been reported [30,31]. The reduction of GO by this method can be readily performed in solutions or on various substrates within seconds. However, the precipitates of $Ti(OH)_4$ after reduction and the TiO_2 nanoparticle products after heat treatment are inevitably left on the surface of the graphene materials, making the preparation of a clean graphene product impossible [30,31]. In this paper, we

* Corresponding author. Tel.: +886 3 2653310; fax: +886 3 2653399.
E-mail address: hongwen@cycu.edu.tw (H.-W. Wang).

0960-1481/$ – see front matter © 2013 Published by Elsevier Ltd.
http://dx.doi.org/10.1016/j.renene.2013.12.001

demonstrate an easy and rapid method for the preparation of both clean graphene materials and TiO_2-graphene composites by using metallic Ti particles in hydrochloride acid solution. When these high quality graphene materials are applied to the flexible TCO-free counter electrode for a dye-sensitized solar cell, comparable or better performances than those using conventional sputtered Pt counter electrode can be obtained.

2. Experimental

2.1. Reagent and materials

Nature graphite powder (Alfa Aesar, >99%, 7–10 micron) was obtained from Sigma–Aldrich U.S.A. and used as received. All other chemicals used in this study were analytical grade (>99%). Titanium powders (60–100 mesh, 99.5%) were purchased from Alfa Aesar, U.S.A. All of the solutions used in this investigation were prepared using de-ionized water (>18 MΩ m).

2.2. Preparation of GO

The GO was prepared by a modified Hummers–Offeman method [7] from natural bulk graphite materials. One gram of graphite was mixed with 0.75 g of Na_2SO_4 and stirred in 30 ml of concentrated sulfuric acid solution. An aliquot of 2.25 g of $KMnO_4$ was added slowly into the mixed solution, and the solution was stirred for 48 h; this was followed by another 2 h of stirring with 300 ml of de-ionized water and 30 ml H_2O_2. After the mixing process, the residuals were washed three times using a 5% HCl aqueous solution and de-ionized water and freeze-dried in high vacuum to give solid GO materials.

2.3. Reduction of GO

GO was prepared as a 0.1 wt.% aqueous solution or ethanolic solution before its reduction. Fifteen milligrams of dried GO solid materials were dispersed ultrasonically in 15 ml of de-ionized water and 15 ml of ethanol, respectively. Four different reduction experiments were conducted in a glass container with a close cover in an oven at a set temperature 120 °C for 3 h, respectively. The solution was slightly boiling during the treatment but not dry out. The products of the reaction were collected by stirring and removing the upper black solution using a glass dropper, as shown in Fig. 1. In this way, the solid metallic Ti particles were easily separated from the solution because they always settled on the bottom. Then, the products were washed in ethanol, centrifuged and dried in an 80 °C oven. Four different experimental solutions were prepared to produce reduced GO (rGO), as follows:

(1). rGO-HCl: 3 ml HCl (37 wt.%) aqueous solution without metallic Ti powder or Ti(III) ions was added to 15 mg GO (aqueous). This acid solution can reduce GO by removing hydroxyl groups.
(2). rGO-water: 50 mg of (60–100 mesh) titanium powders and 3 ml of HCl (37 wt.%) aqueous solution were added to 15 mg of GO (aqueous).
(3). rGO-alcohol: 50 mg of (60–100 mesh) titanium powders and 3 ml of HCl (37 wt.%) aqueous solution were added to 15 mg of GO (ethanolic).
(4). rGO-Ti(III): 50 mg of (60–100 mesh) titanium powders and 3 ml of HCl (37 wt.%) were mixed in 15 ml of de-ionized water and pre-dissolved completely at 120 °C. The clear solution was purple. The Ti metal powder was removed by filtering. Fifteen milligrams of GO were then added to this clear purple solution for reduction. This experiment was performed to confirm whether in-situ-produced Ti(III) ions can reduce GO.

2.4. Instrumentation and measurement

Thermal gravimetric analysis (TGA) and differential thermal gravimetric (DTG) were employed to record the thermal stability of the specimens. TGA scans were performed on a Mettler-Toledo TGA/SDTA851 thermal analysis system in an oxygen atmosphere. The scan rate was 20 °C min^{-1}, and the temperature range was from 30 °C to 700 °C. X-ray diffraction (XRD) was employed to characterize the crystal structure of GO and the graphene materials. The XRD was performed using a Rigaku D/MAX-3C OD-2988N X-ray diffractometer with a Cu target and a Ni filter at a scanning rate of 4° min^{-1} from two theta (2θ) = 20° to 80°. A field emission scanning electron microscope (FESEM, JEOL 7600F) equipped with an energy dispersive spectroscope (EDS, Oxford, 80 nm^2) was used to characterize the morphology and the elemental analysis of GO and rGO-series powders. Transmission electron microscopy (TEM)

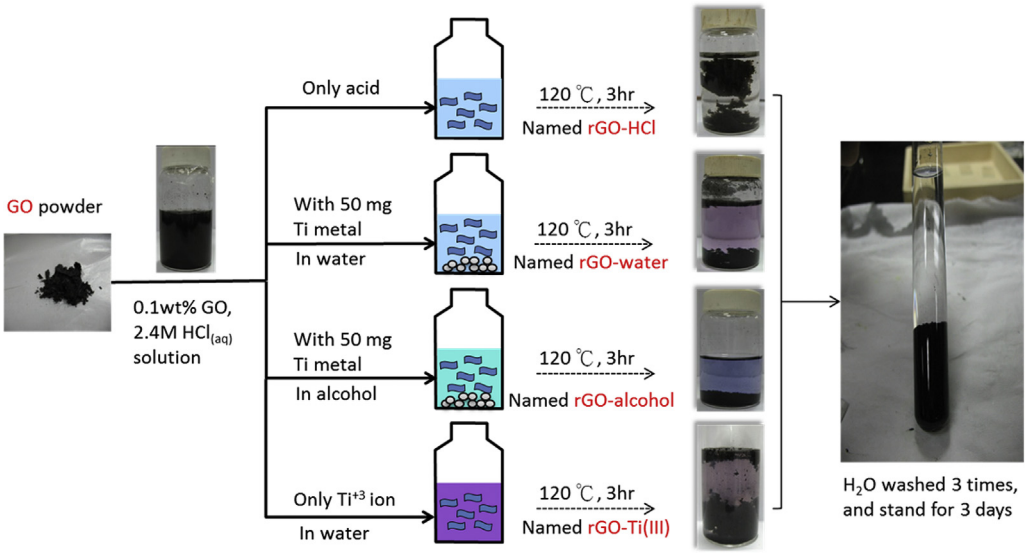

Fig. 1. Four different preparation conditions for rGO.

images and selected area electron diffraction (SAED) patterns were recorded using a JEOL 2010 microscope at an accelerating voltage 200 kV. UV–vis spectra of the GO and reduced GO were obtained using a SHIMADZU UV-2550 spectrophotometer. Fourier transform infrared spectrometry (FTIR) measurements were performed with a JASCO FTIR 460 Plus spectrophotometer. Raman spectral measurements were performed with a JOBIN YVON using a He–Ne laser at a wavelength of 633 nm. X-ray photoelectron spectroscopy (XPS) measurements were performed with a Thermo VG-Scientific Sigma Probe (U.K.) using the energy source Al Kα.

The fabrication of DSSC can be described as followed. A standard TiO_2 photoelectrode was fabricated using a 10 μm thick anatase P25 absorbing layer. An active area of 0.7 cm × 0.7 cm was selected from the TiO_2 electrodes and immersed overnight in a 5×10^{-3} M solution of the dye $[RuL_2(NCS)_2]TBA_2$, where TBA is tetra-n-butylammonium (N719 dye, Everlight Chemical, Taiwan). The active area was covered by the graphene-based counter electrode (rGO-water), which was formed by applying a GO film on a flexible polyimide substrate and subsequently immersing it in the $Ti–Ti^{+3}$ metal-ion co-exited aqueous solution at 120 °C in an oven for 30 min. The GO film is thus reduced. A conventional sputtered Pt-based counter electrode was also prepared for comparison. The "Pt-rGO-water" counter electrode was made by dropping 0.1 ml Pt precursor solution (9 mM in water:EtOH = 2:1 in volume) on the "rGO-water" counter electrode and drying it at 80 °C, followed a quick immersion in 1 M $NaBH_4$ aqueous solution for 5 s. The loading of Pt on graphene is estimated to be less than 10% of the conventional sputtered Pt-based counter electrode. The iodide/triiodide (I^-/I_3^-) electrolyte (Tripod-Technology E-1_MPN) in a quantity of 1 μL was dropped and absorbed into the clamped DSSC assembly. The photovoltaic characteristics of the DSSC devices were measured from an illuminated area of 0.5 cm × 0.5 cm by an electrochemical analyzer (CHI C611B, CH Instruments Co., U.S.A) under standard AM 1.5 sunlight illumination (XES-151S, San-Ei, Japan) with a 100 mW cm^{-2} light source.

3. Results and discussion

3.1. TGA and DTG

The thermal behavior of GO and reduced GO series (rGO-series) up to 700 °C were recorded using TGA, as shown in Fig. 2(A). The removal of the thermally labile oxygen functional groups by chemical reduction results in a much increased thermal stability for

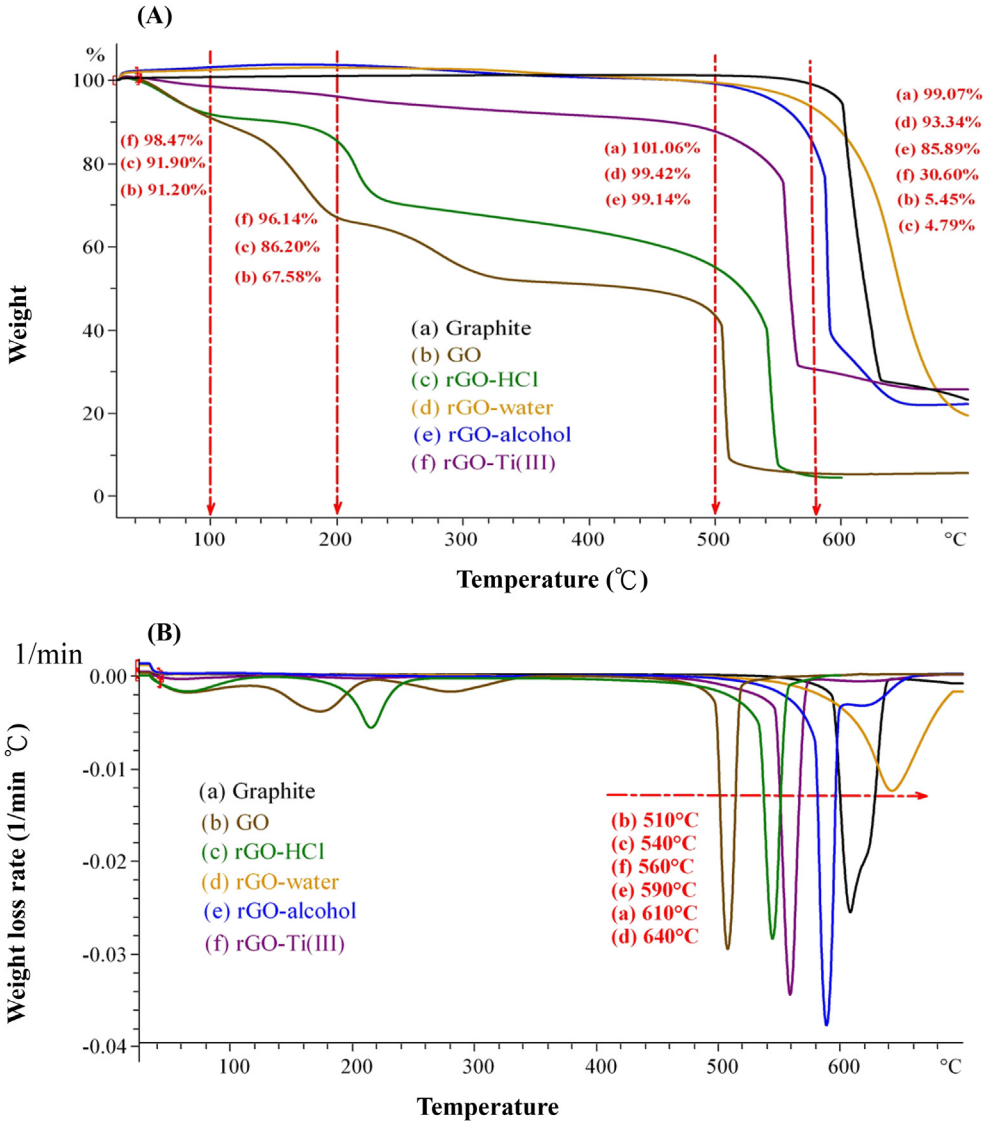

Fig. 2. (A) TGA and (B) DTG of graphite, GO, rGO-HCl, rGO-water, rGO-alcohol and rGO-Ti(III) materials.

the rGO-series. The TGA curves for GO and rGO-HCl exhibit several significant weight losses below 300 °C. The mass loss below 100 °C can be attributed to the loss of adsorbed moisture. The adsorbed moisture was generally resident inside the GO materials due to hydrogen bonding and oxygen-containing functional groups [3]. At 100 °C, the removed mass weights for GO, rGO-HCl, and rGO-Ti(III) were 9%, 6%, 2%, respectively. These values implied that GO, rGO-HCl, and rGO-Ti(III) contained oxygen-containing functional groups. Between 100 and 200 °C, it was expected that the hydroxyl group would be removed. The removal of more stable epoxyl and carbonyl groups occurs at approximately 200–300 °C [8]. According to the curves (b) and (c) in Fig. 2(A), i.e., for the specimen of GO and rGO-HCl, the weight loss was 33% and 12% at 200 °C, respectively. It is clear that the acid solution can significantly remove the hydroxyl groups but not the carbonyl and epoxyl groups. However, when the acid solution contained Ti(III) ions, the removal of carbonyl and epoxyl were obvious, where the curve (f) showed an only 8 wt.% loss at 500 °C. The weight loss of the rGO-Ti(III) system is larger than that of the Ti metal-containing systems below 580 °C, i.e., the rGO-water and rGO-alcohol systems. According to the differential TGA curves (DTG), as shown in Fig. 2(B), it is clear that the thermal stability of rGO-Ti(III) is poorer than that of the rGO-water and rGO-alcohol systems. Notably, the rGO-water (curve (d)) is even more thermally stable than that of graphite (curve (a)) in Fig. 2(B).

3.2. Microscopy analysis

The FESEM morphologies of graphite, GO, rGO-HCl, rGO-Ti(III), rGO-alcohol and rGO-water are shown in Fig. 3(a)–(f), respectively. Through the reduction of Ti–Ti(III) solution, the morphology of GO becomes more loose, as shown in Fig. 3(e), (f). Tiny white particles scattered on the graphene sheets are observed for the rGO-Ti(III) system (Fig. 3(d)) while rGO-water and rGO-alcohol are clean graphene nanosheets. It is the white TiO_2 that makes the color of rGO-Ti(III) powder less dark than that of rGO-water or rGO-alcohol. EDS demonstrated that carbon content was 100% for graphite and that the C/O ratio (59.26/40.74) was 1.45 for GO as the oxygen-containing function groups increased after oxidation, as detailed in Table 1. Reduction using a pristine acid solution only transforms GO into 76.66 at.% carbon and 23.34 at.% oxygen. The results correspond to the TGA plot in Fig. 2(A) curve (c), which shows the

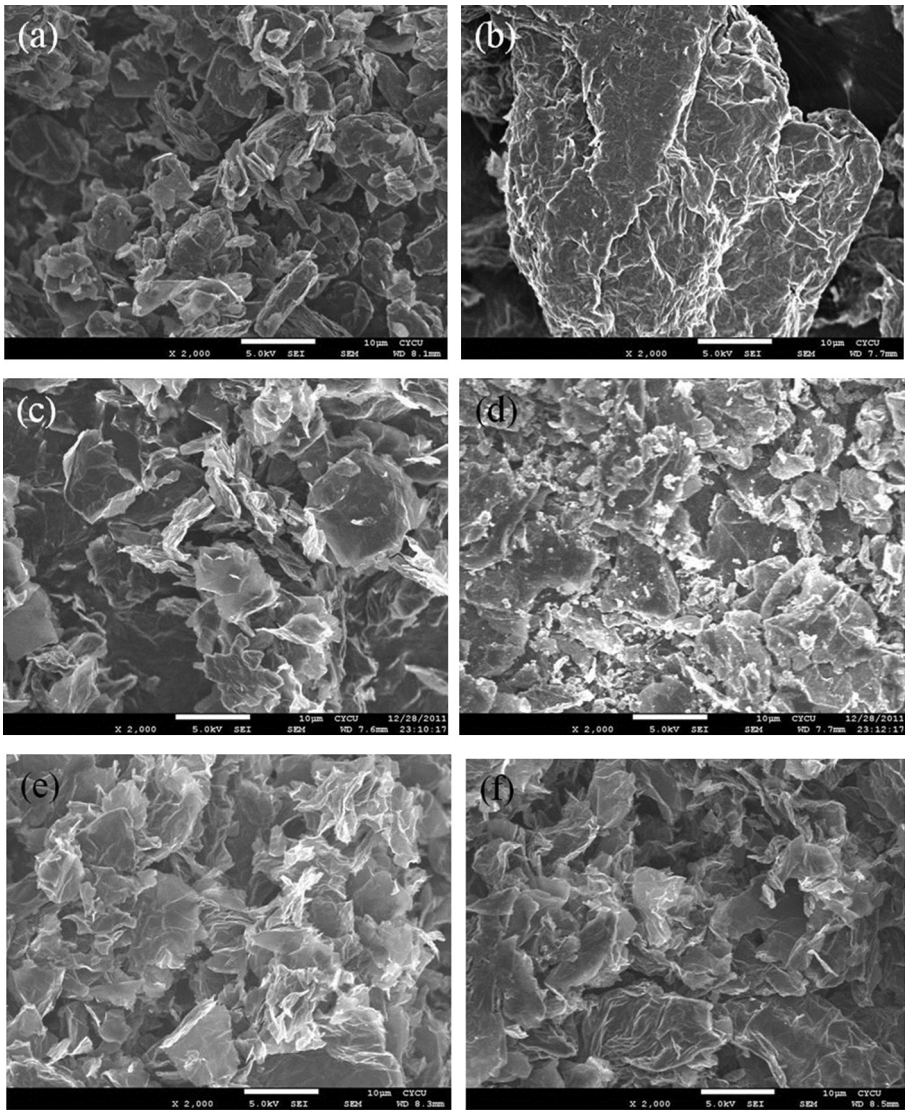

Fig. 3. FESEM of (a) graphite, (b) GO, (c) rGO-HCl, (d) rGO-Ti(III), (e) rGO-water, and (f) rGO-alcohol.

Table 1
EDS analysis for graphite, GO, and various rGO materials.

Sample	C at.%	O at.%	Ti at.%	C/O ratio
Graphite	100%	0%	0%	–
GO	59.26%	40.74%	–	1.45
rGO-HCl	76.66%	23.34%	–	3.28
rGO-water	94.86%	5.14%	–	18.46
rGO-alcohol	93.24%	6.76%	–	13.79
rGO-Ti(III)	80.30%	18.11%	1.59%	4.43

elimination of hydroxyl groups at low temperature (100–200 °C). The introduction of Ti metal in the acid solution increased the carbon content up to 94.86 at.% in water and 93.24 at.% in alcohol, respectively, indicating that the oxygen-containing groups were significantly removed. The atomic ratios of carbon to oxygen are 18.46 and 13.79 for rGO-water and rGO-alcohol, respectively (Table 1). However, when the reduction agent is pristine Ti(III) solution, the carbon content is only 80.30 at.%, which is much less than those of rGO in the Ti–Ti(III) coexisted system. A 1.59 at.% Ti element was also detected by EDS, which was confirmed as TiO_2 in the TEM analysis. Fig. 4(a) and (b) shows the TEM images and the SAED patterns for rGO-Ti(III) and rGO-water, respectively. As evident in the SAED of Fig. 4(a), two distinct phases from graphene and anatase were observed. It was clear that the anatase TiO_2 particles were deposited on the graphene materials. Fig. 4(b) shows the rGO-water system, which is a clean product.

3.3. X-ray diffraction

The XRD patterns are shown in Fig. 5. At the $2\theta = 26.5°$ peak for graphite, the distance was calculated to be 3.35 Å for the (002) interlayers. For the GO (001) peak at $2\theta = 10.3°$, the interlayer distance was calculated to be 8.84 Å. In the meantime, there was a shoulder peak at $2\theta = 20°$, which was considered to be a result of GO layers that were not completely intercalated during oxidation. The increase of the interlayer distance for GO materials was due to the intercalation of oxygen-containing functional groups, which moved the (001) peak to a lower diffraction angle. As the reduction proceeded, the (001) peak moved to a higher diffraction angle at approximately $2\theta = 24.0°$ for those of rGO-water and rGO-alcohol, which are very close to that of graphite. The reduced interlayer distance of the rGO materials was explained because the oxygen-containing functional groups were significantly removed [15,27]. The very broad peaks for the rGO materials implied its amorphous-like nature, which could be understood from FESEM observation. As shown in FESEM (Fig. 3(e), (f)), the loose and irregular morphology of rGOs after the chemical reduction process renders their XRD peaks very broad and of low intensity.

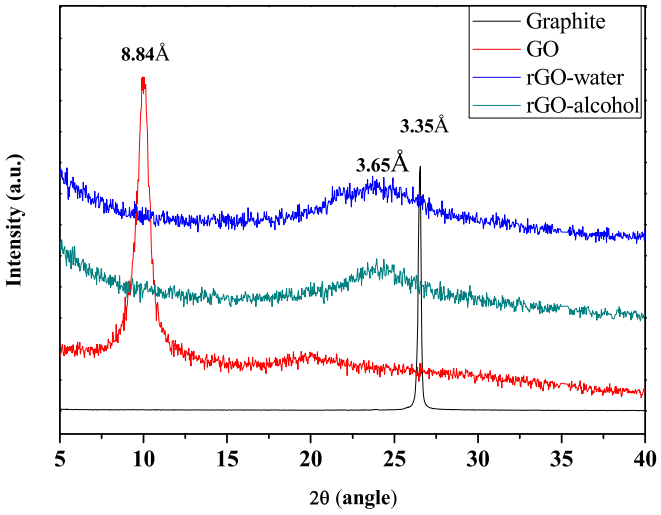

Fig. 5. XRD of graphite, GO, rGO-water, and rGO-alcohol.

3.4. FTIR and UV–vis

Fig. 6 illustrates the FTIR spectra for the graphite, GO, and the reduction of GO using a Ti–Ti(III) coexisted system in water and alcohol. Both rGO-water and rGO-alcohol show good elimination of oxygen-containing functionalities (dotted lines in Fig. 6). In particular, a complete removal of C=O at 1720 cm^{-1} was observed for rGO-water. The UV–vis absorption spectra for the Ti–Ti(III) coexisted system in water shows the typical absorption peaks of Ti(III) ions at 500 nm and its shoulder in the UV–vis spectrum, as shown in Fig. 7. This absorption red-shifted (in web version) slightly to longer wavelengths for Ti–Ti(III) in alcohol. The purple (in web version) Ti(III) ions in water are a strong reducing agent (−1.37 V vs. SHE). The UV–vis absorption spectra for graphite, GO, rGO-water and rGO-alcohol are shown in Fig. 8. A general absorption peak was observed at 230 nm for GO, corresponding to the $\pi \rightarrow \pi^*$ transition of aromatic C–C bonds. Graphite, rGO-alcohol and rGO-water have a remarkable bathochromic $\pi \rightarrow \pi^*$ transition peak at 274 nm, which is very close to the peaks described in the literature [9,17]. The bathochromic peak was due to the restoration of the electronic conjugation of *p* orbitals and thus reduced the required energy for the transition from the highest occupied molecular orbital (HOMO) to the lowest unoccupied molecular orbital (LUMO). The bathochromic peak of the absorption band also implied that the π conjugated systems of rGO-water and rGO-alcohol were significantly recovered [32]. The absorption spectra of GO also showed a carbonyl free electron transition from $n \rightarrow \pi^*$,

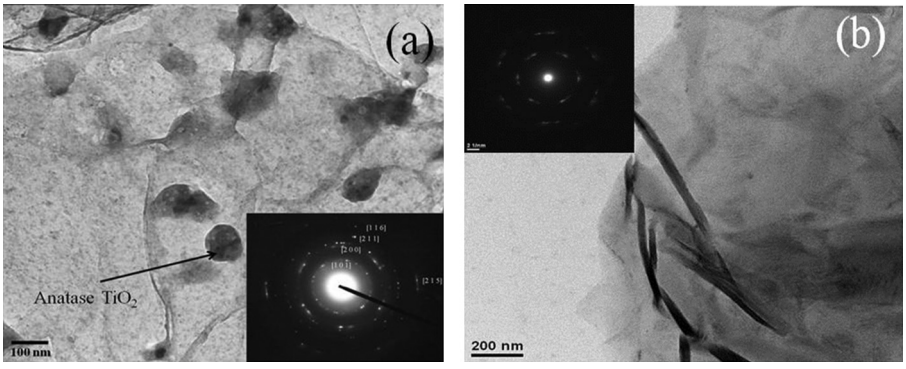

Fig. 4. TEM and SAED (inset) of (a) rGO-Ti(III) and (b) rGO-water.

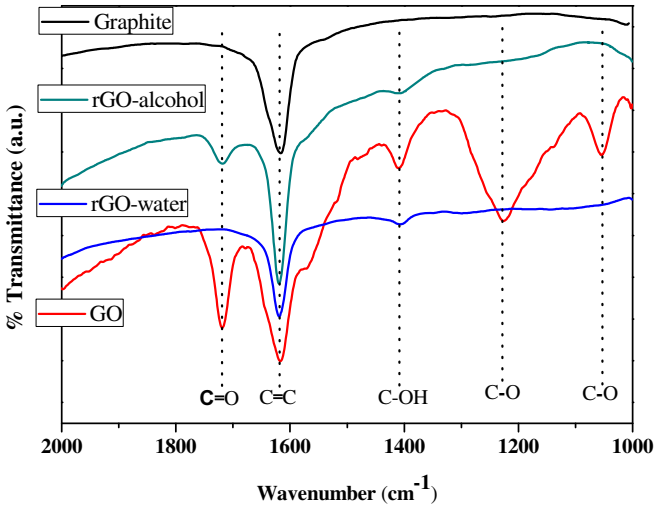

Fig. 6. FTIR of graphite, GO, rGO-alcohol and rGO-water.

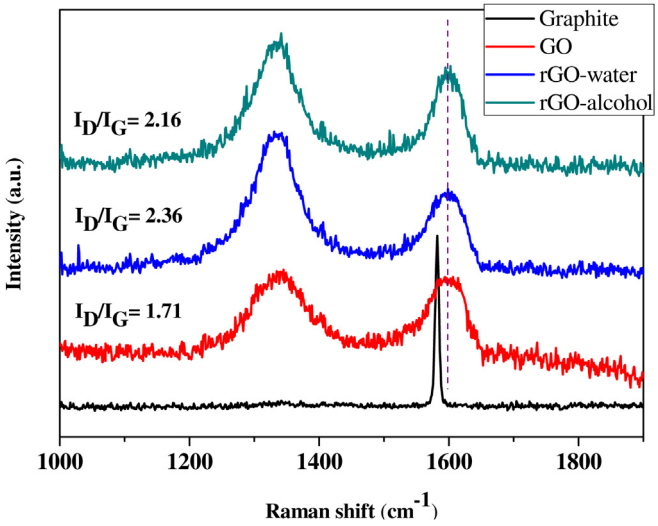

Fig. 9. Raman spectra for graphite, GO, rGO-alcohol and rGO-water.

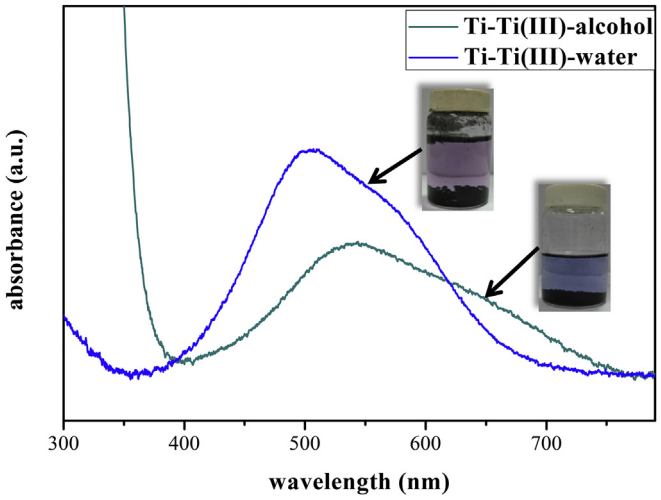

Fig. 7. UV–vis for Ti–Ti(III) in water and Ti–Ti(III) in alcohol.

which was demonstrated at approximately ~300 nm [29,33]. The $n \rightarrow \pi^*$ transition was not observed in graphite and rGO-water but was slightly observed in rGO-alcohol, which implied that the Ti(III) exhibited good reducing ability on carbonyl groups in water but was slightly weaker in alcohol.

3.5. Raman spectra

Raman spectra (Fig. 9) offer another powerful tool for the analysis of structural defects and the disorder of rGO materials. The *G* band at ~1580 cm^{-1} is usually assigned to the E_{2g} mode phonon of sp^2-bonded carbon atoms. The *D* band at ~1350 cm^{-1} is a breathing κ-point phonon of A_{1g} symmetry from a sp^3-bonded carbon atom [34]. These two bands can be observed in defective graphene materials. The Raman spectrum of the graphite displays a strong *G* band at 1580 cm^{-1} while those of GO, rGO-water, and rGO-alcohol all exhibit broadened peaks at the *D* band and the *G* band. The broadened *G* bands are also shifted slightly upward to 1600 cm^{-1} [35]. These broadened peaks are a consequence of disorder after the oxidation and reduction process, which is consisted with the results of XRD pattern in Fig. 5. The I_D/I_G ratio could be

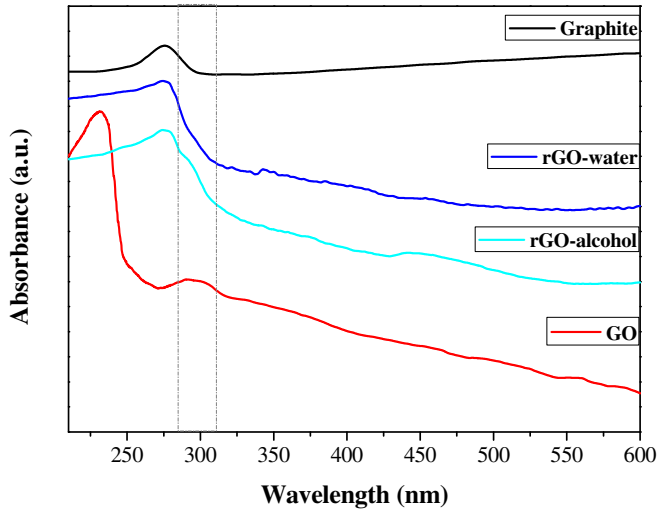

Fig. 8. UV–vis spectrum for graphite, rGO-water, rGO-alcohol, and GO.

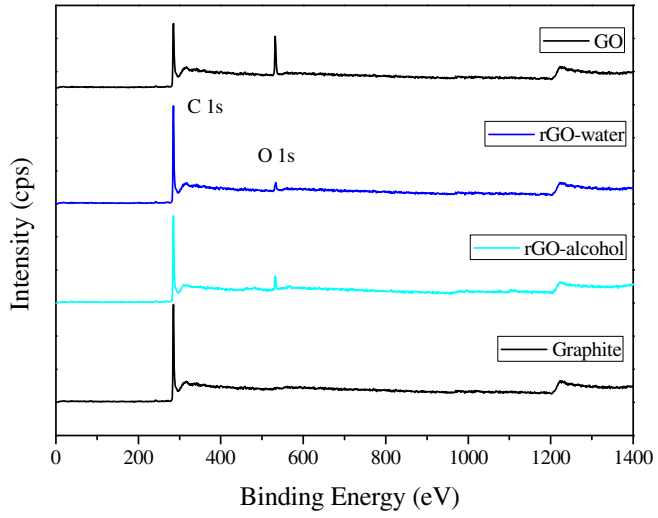

Fig. 10. XPS-survey spectra for GO, rGO-water, rGO-alcohol, and graphite.

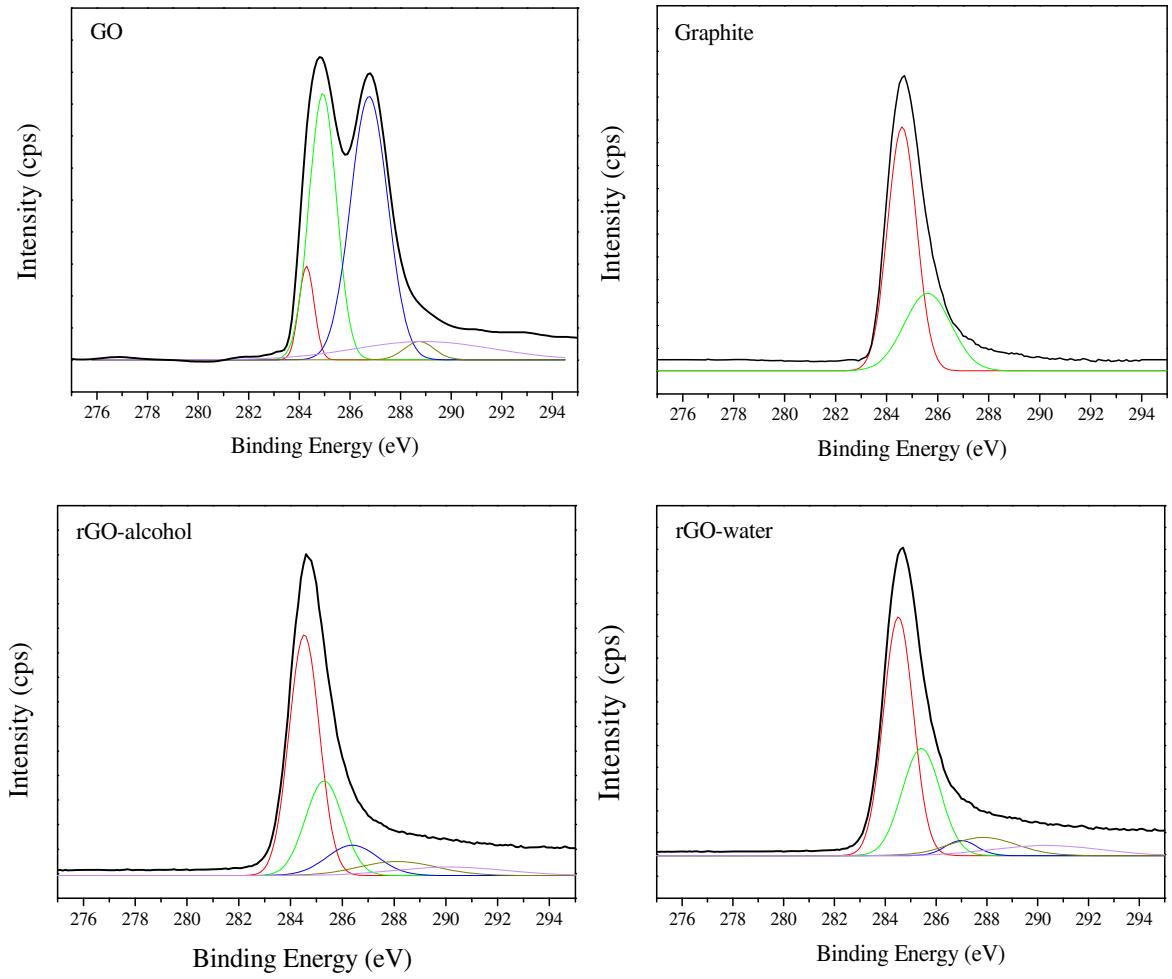

Fig. 11. Chemical state of C1s of GO, graphite, rGO-alcohol, and rGO-water.

used to estimate the sp^2 domain size according to the Tuinstra–Koenig relation. The I_D/I_G ratio of GO was 1.71, and those of rGO-water and rGO-alcohol were 2.36 and 2.16, respectively. The increased I_D/I_G ratio could be a consequence of a high number of defects in the rGO materials, which was also observed by other studies [7,9]. The reduced average size of the sp^2-domains can increase the I_D/I_G ratio, i.e., an increased number of small domains of aromaticity (responsible for the *D* peak), but not necessarily their overall size, which is responsible for the *G* peak [10,20]. In our experiments, the use of ultrasonic dispersion to produce a suspension of GO might break down the graphene structure, resulting in a small sp^2-domain size.

3.6. XPS

Figs. 10 and 11 show the XPS results for GO, graphite, rGO-water, and rGO-alcohol. It is clear that the oxygen peak is almost eliminated. The detailed deconvoluted spectrum of GO gives five peaks at 284.5, 285.6, 286.7, 287.8, and 288.8 eV from the C1s peak, which correspond to C–C (sp^2), C–C (sp^3), C–O, C=O, and O–C=O, respectively [36]. The decreases of the oxygen-containing functionalities are significant, as detailed in Table 2. The C/O ratio increases from 1.34 for GO to 23.44 for rGO-water and 15.78 for rGO-alcohol. Moreover, no signature for Ti or its chemical state was observed in the EDS and XPS analysis, confirming that rGO-water and rGO-alcohol are completely free of TiO_2.

3.7. Formation mechanism of TiO_2 on graphene

Why did the rGO-water and rGO-alcohol systems not produce TiO_2 nanoparticles? As shown in Fig. 12, when saturated Ti(III) was present in the solution, they exhibited higher affinity to the oxygen-containing groups, reduced them and became soluble Ti(IV) hydroxo complexes, $Ti(OH)^{+3}$ or $Ti(OH)_n^{+(4-n)}$ ions [37,38]. When Ti metal was still present in the solution, the supply of Ti(III) was sufficient due to the continuous dissolution of metallic Ti. The

Table 2
Fitting of the C1s peak binding energy (eV) (relative %) and C/O atomic ratio.

	C–C sp^2	C–C sp^3	C–O	C=O	C–O=C	C/O
Graphite	284.5 (67.43)	285.6 (33.56)	–	–	–	–
GO	284.5 (6.84)	285.6 (28.75)	286.7 (34.73)	287.8 (25.64)	288.8 (4.04)	1.34
rGO-water	284.5 (50.89)	285.6 (29.30)	286.7 (3.38)	287.8 (8.66)	288.8 (7.5)	23.44
rGO-alcohol	284.5 (50.69)	285.6 (24.56)	286.7 (10.8)	287.8 (7.74)	288.8 (6.42)	15.78

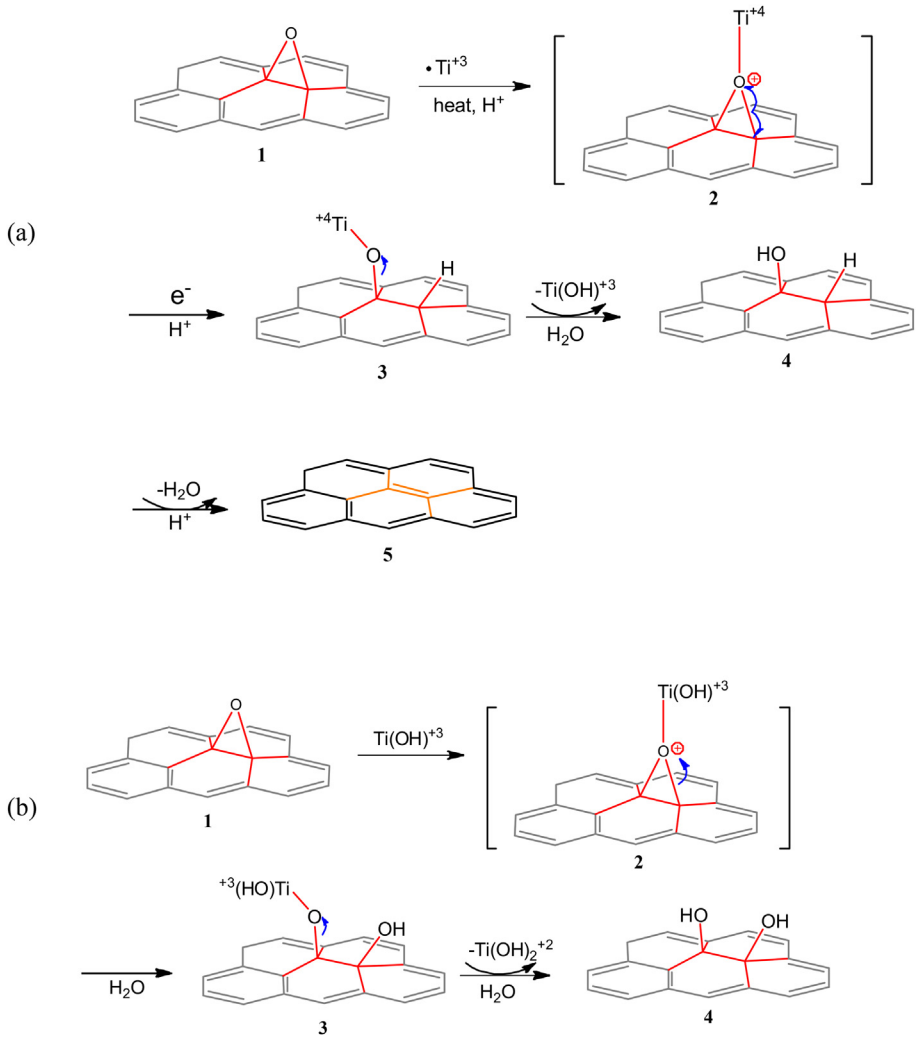

Fig. 12. Mechanisms for the formation of graphene through the removal of (a) epoxyl when Ti–Ti(III) coexists and the supply of Ti(III) is unlimited and (b) epoxyl when only Ti(III) is used and becomes limited.

reduction of oxygen-containing groups will always put Ti(III) ions in the first priority. The oxidation of Ti(III) gives many other soluble hydroxo complexes of Ti(IV), such as $Ti(OH)^{+3}$, $Ti(OH)_2^{+2}$, etc. These soluble ions will be easily washed off, resulting in a clean graphene product. The formation of TiO_2 on the rGO-Ti(III) system could be due to the oxidation of Ti(III) to Ti(IV) hydroxides, $Ti(OH)_4$. The absence of Ti metal in the Ti(III) solution will lead to a diminished concentration of Ti(III) and compel $Ti(OH)^{+3}$ ions to continually reduce the GO and oxidize (Fig. 12(b)). Eventually, $Ti(OH)^{+3}$ or $Ti(OH)_2^{+2}$ will become $Ti(OH)_4$, a solid precipitate, formed on the graphene nanosheets (Figs. 3(d) and 4(a)). The outcome of Fig. 12(b) also coincides with the slight weight loss between 100 °C and 200 °C in the TGA plot (Fig. 2(f) curve).

3.8. Application of rGO-water as the counter electrode

According to the analysis above, rGO-water is proved to be a high quality graphene material, and its application to replace the conventional Pt-based counter electrode of dye-sensitized solar cells (DSSCs) was a success. These graphene nanosheets, which possess a high C/O ratio, exhibit high surface conductivity (~10 Ω/sq) when they are reformed into films on a flexible polyimide substrate. The DSSC using the rGO-water counter electrode exhibits a photoelectric conversion efficiency of 5.45% compared to 5.52% for the Pt counter electrode on the same DSSC, as shown in Fig. 13 and Table 3. The general performance of DSSC using this high quality graphene as a flexible counter electrode normally achieves ≥98% of the performance when using a conventional Pt-based counter

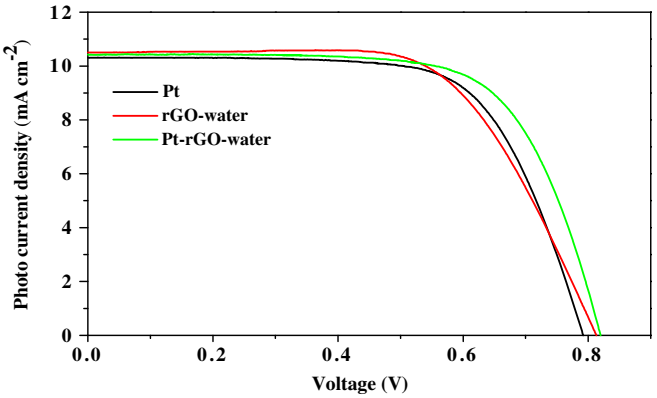

Fig. 13. *J–V* curve for DSSCs based on the counter electrodes of conventional sputtered Pt, graphene (rGO-water) and Pt nanoparticle incorporated graphene (Pt-rGO-water).

Table 3
Performance data of DSSC based on the counter electrodes of Pt and rGO-water.

Counter electrode	V_{oc} (mV)	J_{sc} (mA)	Conversion (%)	FF	Rs (Ω)
Pt	792	10.31	5.52	0.676	17.23
rGO-water	813	10.54	5.45	0.636	16.64
Pt-rGO-water	819	10.43	5.87	0.687	17.98

electrode. With the incorporation of Pt nanoparticles on the rGO-water counter electrode (refer as "Pt-rGO-water"), which is described in experiment section, the FF and the conversion efficiency is improved, resulting in a better performance ($\eta = 5.87\%$) than that of the Pt-based counter electrode, though the J_{sc} and V_{oc} have not changed much. The enhancement of the FF may be attributed to the facilitated reduction of I_3^- ions, which is caused by the incorporated Pt nanoparticles on the graphene surface. The replacement of the Pt/FTO/glass rigid counter electrode with the current graphene/PI or Pt-incorporated graphene/PI flexible counter electrode requires easy processing conditions with neither heat treatment at high temperature nor a FTO buffer layer; however, it enables an excellent alternative for versatile DSSCs with the need of no or very little Pt metal loading ($\leq$10%).

4. Conclusion

We have demonstrated a novel, easy and scalable method to synthesize high quality graphene nanosheet powders. The Ti(III) is dissociated from metallic Ti particles in an acid environment and effectively reduces the oxygen-containing functional groups of GO. When the supply of Ti(III) is sufficient, the species with Ti(IV) hydroxo complexes such as $Ti(OH)^{+3}$, $Ti(OH)_2^{+2}$ are soluble and easily washed off. When the supply of Ti(III) is limited, the final form after the reduction process, $Ti(OH)_4$ precipitates, inevitably stay in the solution. The baking of these precipitates at 80 °C resulted in anatase TiO_2 nanocrystals. By using metal titanium in hydrochloride acid solution, we are able to synthesize a graphene with graphitic characteristics that are comparable to those of pristine graphite. These graphene nanosheets, which possess a high C/O ratio and a high surface conductivity, enable an excellent flexible TCO-free counter electrode for use in DSSCs.

Acknowledgments

This work was supported financially by the National Science Council, Taiwan (NSC99-2113-M-033-003–MY3).

References

[1] O'Regan B, Grätzel M. A low-cost, high-efficiency solar cell based on dye-sensitized colloidal TiO_2 films. Nature 1991;353:737–40.
[2] Singh V, Joung D, Zhai L, Das S, Khondaker SI, Seal S. Graphene based materials past, present and future. Prog Mater Sci 2011;56:1178–271.
[3] Dreyer DR, Park S, Bielawski CW, Ruoff RS. The chemistry of graphene oxide. Chem Soc Rev 2010;39:228–40.
[4] Novoselov KS, Geim AK, Morozov SV, Jiang D, Zhang Y, Dubonos SV, et al. Electric field effect in atomically thin carbon films. Science 2004;306:666–9.
[5] Hummers WS, Offeman RE. Preparation of graphitic oxide. J Am Chem Soc 1958;80:1139.
[6] Stankovich S, Dikin DA, Piner RD, Kohlhaas KA, Kleinhammes A, Jia Y, et al. Synthesis of graphene -based nanosheets via chemical reduction of exfoliated graphite oxide. Carbon 2007;45:1558–65.
[7] Ai K, Liu Y, Lu L, Cheng X, Huo L. A novel strategy for making soluble reduced graphene oxide sheets cheaply by adopting an endogenous reducing agent. J Mater Chem 2011;21:3365–70.
[8] Kaniyoor A, Baby TT, Arockiadoss T, Rajalakshmi N, Ramaprabhu S. Wrinkled graphenes: a study on the effects of synthesis parameters on exfoliation-reduction of graphite oxide. J Phys Chem C 2011;115:17660–9.
[9] Xu Y, Sheng K, Li C, Shi G. Highly conductive chemically converted graphene prepared from mildly oxidized graphene oxide. J Mater Chem 2011;21:7376–80.
[10] Stankovich S, Dikin DA, Dommett GHB, Kohlhaas KM, Zimney EJ, Stach EA, et al. Graphene-based composite materials. Nature 2006;442:282–6.
[11] Tung VC, Chen LM, Allen MJ, Wassei JK, Nelson K, Kaner RB, et al. Low-temperature solution processing of graphene-carbon nanotube hybrid materials for high-performance transparent conductors. Nano Letters 2009;9:1949–55.
[12] Wang GX, Shen XP, Yao J, Park J. Graphene nanosheets for enhanced lithium storage in lithium ion batteries. Carbon 2009;47:2049–53.
[13] Wang GX, Yang J, Park J, Gou XL, Wang B, Liu H, et al. Facile synthesis and characterization of graphene nanosheets. J Phys Chem C 2008;112:8192–5.
[14] Dreyer DR, Murali S, Zhu YW, Ruoff RS, Bielawski CW. Reduction of graphite oxide using alcohols. J Mater Chem 2011;21:3443–7.
[15] Sheng Z, Yuyan S, Honggang L, Mark HE, Geping Y, Yuehe L. Polyelectrolyte-induced reduction of exfoliated graphite oxide: a facile route to synthesis of soluble graphene nanosheets. ACS Nano 2011;5:1785–91.
[16] Jincheng L, Huiseong J, Jinzhang L, Kyungmoon L, Ji-Yong P, Ahn YH, et al. Reduction of functionalized graphite oxides by trioctylphosphine in non-polar organic solvents. Carbon 2010;48:2282–9.
[17] Fernández-Merino MJ, Guardia L, Paredes JI, Villar-Rodil S, Solís-Fernández P, Martínez-Alonso A, et al. Vitamin C is an ideal substitute for hydrazine in the reduction of graphene oxide suspensions. J Phys Chem C 2010;114:6426–32.
[18] Ken-Hsuan L, Anudha M, Shameek B, Christopher L, Mkhoyan KA, Christopher WM. Aqueous only route toward graphene from graphite oxide. ACS Nano 2011;5:1253–8.
[19] Xiaobin F, Wenchao P, Yang L, Xianyu L, Shulan W, Guoliang Z, et al. Deoxygenation of exfoliated graphite oxide under alkaline conditions: a green route to graphene preparation. Adv Mater 2008;20:4490–3.
[20] Ding YH, Zhang P, Zhuo Q, Ren HM, Yang ZM, Jiang Y. A green approach to the synthesis of reduced graphene oxide nanosheets under UV irradiation. Nanotechnology 2011;22:215601–6.
[21] Chen C, Chen T, Wang H, Sun G, Yang X. A rapid, one-step, variable-valence metal ion assisted reduction method for graphene oxide. Nanotechnology 2011;22:405602–8.
[22] Zhou X, Huang X, Qi X, Wu S, Xue C, Boey FYC, et al. In situ synthesis of metal nanoparticles on single-layer graphene oxide and reduced graphene oxide surfaces. J Phys Chem C 2009;113:10842–6.
[23] Wang S, Jiang SP, Wang X. Microwave-assisted one-pot synthesis of metal/metal oxide nanoparticles on graphene and their electrochemical applications. Electrochim Acta 2011;56:3338–44.
[24] Moussa S, Atkinson G, Samy-Shall M, Shehata A, Abou-Zeidb KM, Mohamed MB. Laser assisted photocatalytic reduction of metal ions by graphene oxide. J Mater Chem 2011;21:9608–19.
[25] Chen Q, Zhang L, Chen G. Facile preparation of graphene-copper nanoparticle composite by in situ chemical reduction for electrochemical sensing of carbohydrates. Anal Chem 2012;84:171–8.
[26] Dey RS, Hajra S, Sahu RK, Raj CR, Panigrahi MK. A rapid room temperature chemical route for the synthesis of graphene: metal-mediated reduction of graphene oxide. Chem Commun 2012;47:1787–9.
[27] Fan ZJ, Kai W, Yan J, Wei T, Zhi LJ, Feng J. Facile synthesis of graphene nanosheets via Fe reduction of exfoliated graphite oxide. ACS Nano 2011;5:191–8.
[28] Xue Y, Chen H, Yu D, Wang S, Yardeni M, Dai Q, et al. Oxidizing metal ions with graphene oxide: the in-situ formation of magnetic nanoparticles on self-reduced graphene sheets for multifunctional applications. Chem Commun 2011;47:11689–91.
[29] Gotoh K, Kinumoto T, Fujii E, Yamamoto A, Hashimoto H, Ohkubo T, et al. Exfoliated graphene sheets decorated with metal/metal oxide nanoparticles: simple preparation from cation exchanged graphite oxide. Carbon 2011;49:1118–25.
[30] Chengzhou Z, Shaojun G, Ping W, Li X, Youxing F, Yueming Z, et al. One-pot, water-phase approach to high-quality graphene/TiO_2 composite nanosheets. Chem Commun 2010;46:7148–50.
[31] Xiang G, He J, Li T, Zhuang J, Wang X. Rapid preparation of noble metal nanocrystals via facile coreduction with graphene oxide and their enhanced catalytic properties. Nanoscale 2011;3:3737.
[32] Li D, Mueller MB, Gilje S, Kaner RB, Wallace GG. Processable aqueous dispersions of graphene nanosheets. Nat Nanotechnol 2008;3:101–5.
[33] Eda G, Lin YY, Mattevi C, Yamaguchi H, Chen HA, Chen IS, et al. Blue photoluminescence from chemically derived graphene oxide. Adv Mater 2010;22:505–9.
[34] Nemanich RJ, Solin SA. First- and second-order raman scattering from finite–size crystals of graphite. Phys Rev B 1979;20:392–401.
[35] Tuinstra F, Koenig JL. Raman spectrum of graphite. J Chem Phys 1970;53:1126–30.
[36] Sui Z, Zhang X, Lei Y, Luo Y. Easy and green synthesis of reduced graphite oxide-based hydrogels. Carbon 2011;49:4314–21.
[37] Wang TH, Navarrete-López AM, Li S, Dixon DA, Gole JL. Hydrolysis of $TiCl_4$: initial steps in the production of TiO_2. J Phys Chem A 2010;114:7561–70.
[38] Sugimoto T, Zhou X, Collo AJ. Synthesis of uniform anatase TiO_2 nanoparticles by gel–sol method solution chemistry of $Ti(OH)_{(4-n)}^{+n}$ complexes. J Colloid Interface Sci 2002;252:339–46.